A Real-Time Simultaneous Small- and Wide-Angle X-ray Scattering Study of *in Situ* Polyethylene Deformation at Elevated Temperatures

Michael F. Butler[†] and Athene M. Donald*

Department of Physics, Cavendish Laboratory, University of Cambridge, Madingley Road, Cambridge CB3 0HE, U.K.

Received May 15, 1997; Revised Manuscript Received October 3, 1997

ABSTRACT: A variety of polyethylenes were investigated over a range of drawing temperatures by the simultaneous measurement of the small- and wide-angle X-ray scattering patterns and the load−extension curve and were all found to undergo a similar sequence of deformation processes under 90 °C. Interlamellar separation was identified during preyield deformation. Crystallographic deformation via chain slip and a temperature- and crystallinity-dependent martensitic phase transformation were associated with macroscopic yielding in all cases. The lamellar to fibrillar transition occurred immediately after yielding as the load dropped. Once the load became constant, the fibrillar morphology had fully formed. Deformation of the microfibrils was detected during the load−extension curve plateau. The percentage crystallinity was the most important influence on the mechanical response whereas branch length had no effect. Above 90 °C, it was speculated that a greater amount of interlamellar deformation was activated in the less crystalline linear low-density polyethylene (LLDPE), and this accounted for the differences in mechanical behavior between LLDPE and high-density polyethylene (HDPE) above this temperature.

1. Introduction

Polyethylene (PE) is a semicrystalline polymer, the study of which continues to be of much interest. Its mechanical properties are particularly important owing to its use in many applications where load-bearing ability is essential. Tailoring the molecular architecture by including short chain side branches to form linear low-density polyethylene (LLDPE) has been found to be a means of altering the mechanical properties.[1] In this paper, data are presented from both high-density PE (HDPE), which contains no side chain branches, and LLDPE drawn at elevated temperatures. Other influences (branch type, molecular weight and thermal history) are also considered in order to present a more comprehensive picture on the factors affecting the deformation mechanisms active in initially unoriented PE.

The operation of a variety of deformation processes has been reported in the extensive literature dealing with the mechanical properties of PE. Lamellar separation, shear and rotation, chain slip, twinning, and a martensitic transformation are the most prevalent mechanisms, and evidence for their occurrence has been summarized most recently in the review by Lin and Argon.[2] It is generally accepted that interlamellar deformation mechanisms, involving the rubbery amorphous component, are dominant during the initial stages of deformation but that yielding results from crystallographic deformation.[3,4] The drawing temperature is expected to be important, since many of the deformation mechanisms are temperature dependent. Interlamellar shear is known to be enhanced at temperatures above 80 °C,[5,6] whereas the martensitic transformation is suppressed.[7] In the dislocation model of crystallographic deformation, higher temperatures increase both the number of dislocations generated and their mobility, thus enhancing the amount of chain slip.[8] In addition, 70 °C is above the α relaxation temperature, at which the crystals become weaker and more disposed to shear.[9−13] An increase in the thermal expansion of the crystalline unit cell may also increase the chain mobility in the crystalline phase, enhancing the ease of chain slip.[14,15] In the alternative melting and recrystallization model, where the heat of deformation causes partial melting and subsequent oriented recrystallization,[16−21] an increased drawing temperature lowers the temperature differential between molten and solid phases, thus making deformation easier.

As a consequence of deformation the lamellar microstructure of PE is converted into an oriented fibrillar one,[20] although the precise mechanism for the transition still remains uncertain. Both crystallographic deformation by mechanical rearrangement of the lamellae as well as melting and recrystallization have been used to describe the process. It is believed that a combination of these two processes may occur, with the mechanical mechanism dominating at lower temperatures[20,22−24] and melting and recrystallizing increasing in importance with increasing temperature.[25−27]

Real-time simultaneous measurement of the small- and wide-angle X-ray scattering (SAXS and WAXS respectively) during *in situ* deformation presents two advantages over previous *ex situ* studies of the deformation processes in semicrystalline polymers. First, the high flux of X-rays produced by a synchrotron radiation source allows real-time *in situ* experiments to be performed. The consequent elimination of sample relaxation enables accurate, unambiguous information about the microstructure in the deforming state to be obtained. Second, the use of two area detectors enables changes on both lamellar (via SAXS) and molecular (via WAXS) length scales to be precisely correlated. In addition, the collection of the load−extension curve in

[†] Present Address: Department of Materials Science and Metallurgy, University of Cambridge, New Museums Site, Pembroke Street, Cambridge, CB2 3QZ, UK.

* To whom correspondence should be addressed. Telephone: (+44) (0)1223 337007. Fax: (+44) (0)1223 337000.

S0024-9297(97)00681-5 CCC: $15.00
Published on Web 08/15/1998

Table 1. Sample Information

sample	M_w/1000	M_w/M_n	SCB[a]/1000C	SCB[a] type
		HDPE		
A	60	4.7	<2.0	butyl
B	131	6.3	<0.5	butyl
		HMW−HDPE		
E	385	9.0	0	N/A
		LLDPE		
G	152	5.2	23.7	ethyl
H	126	4.2	21.0	isobutyl
I	110	3.0	∼20	butyl

[a] SCB = short chain branch.

conjunction with the SAXS and WAXS patterns allows the macroscopic deformation to be directly related to the microscopic deformation.

2. Experimental Section

2.1. Materials and Sample Preparation. A range of high density, high molecular weight high density and linear low-density polyethylenes (HDPE, HMW−HDPE, and LLDPE, respectively), supplied by BP Chemicals Ltd., were used in this study. The PE grades were selected to provide a series of samples possessing different molecular weights, densities, branch types, and branch amounts. Sample information is summarized in Table 1.

Plaques, 0.9 mm thick, were formed by compression-molding the molten PE using the method described previously.[28] Specially shaped samples for tensile testing in the X-ray beam were punched from these plaques. They were 50 mm long and 20 mm wide, with two semicircular cutouts of radius 8 mm to ensure that yielding always occurred in the beam.

Some of the HDPE and HMW−HDPE samples were annealed in a vacuum at 132 ± 1 °C for 22 h and some of the LLDPE samples at 113 ± 1 °C in order to change their percentage crystallinities, lamellar thicknesses and lamellar populations. They were then cooled slowly (initial cooling rate 0.5 °C/min) to room temperature. Annealed samples are denoted by SC, and the unannealed ones by U, to match the previous notation.[28]

2.2. Differential Scanning Calorimetry. Differential scanning calorimetry (DSC) was used to obtain the percentage crystallinity of the samples and information on the lamellar populations and thicknesses, from both undeformed material and from sections cut from the deformed regions (after sample relaxation) of the specimens studied using SAXS and WAXS. Measurements were taken on a Perkin-Elmer DSC7 equipped with an Intracooler II and calibrated with indium and zinc. The heating rate used was 10 °C/min.

The lamellar thickness, L_c, was estimated by rearranging the equation for the melting point, T_m.

$$L_c = \frac{2\sigma_e}{\Delta h}\frac{T_{m0}}{(T_{m0} - T_m)} \tag{1}$$

Using the value of (93 ± 8) × 10^{-7} J/cm^2 for the fold surface energy, σ_e,[29] employing 280 J/cm^3 for the heat of fusion of crystal, Δh,[29] and taking the equilibrium melting temperature, T_{m0}, to be equal to 145.8 °C,[29] lamellar thicknesses were estimated. The percentage crystallinity was calculated from the specific heat of fusion by taking the specific heat of fusion of perfectly crystalline PE to be 293 J/g.[30]

2.3. Simultaneous SAXS/WAXS Measurement during *in Situ* Deformation. X-ray scattering experiments were performed on beamline 16.1[31,32] at the Synchrotron Radiation Source (SRS), Daresbury, U.K. The same experimental setup as that described and illustrated previously was used.[28,33] Two-dimensional SAXS and equatorial WAXS patterns were obtained from the central highly deformed region of the sample simultaneously during deformation, using two gas-filled multiwire area detectors. Drawing proceeded at an extension rate of 5.0 mm/min in a computer-controlled Rheometrics Ltd. Miniature Materials Tester equipped with an environmental chamber for the purpose of performing experiments at elevated temperatures. Mica windows enabled X-rays to pass through the chamber. Samples were deformed at 20, 40, 70, 90, and 110 °C. The load−extension curve and the X-ray scattering patterns were obtained simultaneously. Owing to the complicated sample shape, however, neither the stress nor the local strain could be easily measured. It is therefore vital to appreciate that, although the nominal strain is used in the subsequent results and discussion, the local strain may have been quite different in the region where the X-rays were targeted since the relationship between extension and local strain will be highly nonlinear. This problem is considered further in the dicussion section.

The Lorentz correction,[34,35] which corresponds to multiplying the intensity by q^2, where **q** is the scattering vector, was applied to all of the SAXS data resulting from a lamellar morphology. The scattering vector is taken to be

$$|\mathbf{q}| = q = \frac{2\pi}{d} = \frac{4\pi}{\lambda}\sin\theta \tag{2}$$

where d is the long spacing, λ the X-ray wavelength, and θ the scattering angle. The Lorentz correction is necessary in a randomly oriented sample to correct for the different probabilities of planes being in the reflection condition. In applying this correction the assumption is made that the lamellae are randomly oriented throughout the whole sample. Since this is correct for undeformed PE but not so when the structure has become fibrillar, the SAXS data from the fibrillar morphology were left unaltered for the purpose of calculating fiber long spacings.

To compensate for fluctuations in incident beam intensity, both small- and wide-angle scattering data were normalized with respect to readings on ion counters placed in front of and behind the sample. Corrections were made for sample thickness, sample transmission, and detector nonlinearity. The background scattering was subtracted from both the SAXS and WAXS data. There was no need to desmear the data due to the point collimated size of the beam compared with the pixel size of the detectors. The channel numbers of the small-angle area detector were calibrated using wet rat-tail collagen.

Owing to limitations imposed by the use of a gas-filled detector, no quantitative information regarding peak widths or azimuthal widths could be obtained for the WAXS data. Analysis was therefore confined to the calculation of peak intensities, as a general indication of the changes in the equatorial portion of the WAXS pattern, and the identification of phases present.

3. Results

3.1. Tensile Behavior. HDPE and HMW−HDPE samples deformed inhomogeneously with the formation of stable necks at all temperatures whereas the LLDPE samples tended to deform homogeneously above 90 °C and inhomogeneously below 90 °C. In the case of the LLDPEs, a distinct yield point was not observed above 70 °C. With the exception of annealed HDPE sample A, all of the samples were ductile. In the samples that deformed inhomogeneously, a drop in the load was registered after the yield point. It should be emphasized that this drop does not necessarily signify the occurrence of strain-softening. In the homogeneously deforming samples no load drop was registered.

The appearance of the neck was affected by the drawing temperature, especially in the case of the HDPE and HMW−HDPE samples. The necked region of HDPE samples at temperatures below 70 °C was white. This whitening could be correlated with the formation of voids indicated by the SAXS pattern (described later). Cavitation was absent at higher temperatures, however, and the neck became clearer

Table 2. Trends Shown by DSC: The Influence of Drawing Temperature upon the Melting Point and Percentage Crystallinity of Drawn Samples Compared to Undrawn Ones

sample type	melting point	percentage crystallinity
HDPE, HMW−HDPE	increases with increasing drawing temperature	low-temperature cavitated samples: less than undeformed material; decreases more with decreasing temperature.
		high temperature noncavitated samples: greater than undeformed material; increases with increasing temperature.
LLDPE	increases with increasing drawing temperature	all temperatures: greater than undeformed material; increases with increasing temperature

than the undeformed material. LLDPE samples did not cavitate at any temperature, and the necked region in all cases was clearer than the undeformed material.

3.2. DSC. Table 2 summarizes the influence of drawing temperature on the melting point and the percentage crystallinity of the different samples. The detailed values are given elsewhere.[36] The trends in percentage crystallinity with temperature were more marked for the homopolymer samples (i.e. the HDPE and HMW−HDPE) than for the LLDPE (copolymer) samples. Two separate classes of behavior were observed for the HDPE, depending on whether cavitation had occurred or not. Uncavitated deformed samples possessed a higher percentage crystallinity than the undeformed material. Cavitated HDPE, on the other hand, was less crystalline than the undeformed material. The decrease in percentage crystallinity lessened, however, with increasing drawing temperature.

3.3. WAXS. Sequences of equatorial WAXS patterns from unannealed HDPE sample B taken at 70 and 110 °C, together with the simultaneously obtained SAXS patterns and load−extension curves, are shown in parts a and b of Figure 1, respectively. Similar patterns were obtained for all of the other samples. Drawing at 40 °C produced similar results to those found in cold-drawn samples, which have been described elsewhere,[33,37] whereas drawing at 90 °C was similar to that at 110 °C. Extra reflections, identified as resulting from the monoclinic phase, appeared at the yield point for all of the samples drawn at 20 and 40 °C and in the annealed HDPE and both annealed and unannealed HMW−HDPE samples drawn at 70 °C. The behavior of the monoclinic reflections was identical to that of the cold-drawn HDPE and LLDPE samples described in more detail previously.[33,37]

It can be seen from Figure 1 that the WAXS registered an increasing molecular orientation as the samples were drawn. No appreciable orientation was observed (by detailed inspection of the WAXS pattern at different contrast levels) prior to the yield point, however. The orthorhombic (200) reflection oriented toward the equator first, followed by the orthorhombic (110) and (020) and the monoclinic reflections when present. At all temperatures for the HDPEs and HMW−HDPEs the orthorhombic (110) reflection became oriented via a four-point pattern which persisted during the drop in load after yielding and into the load−extension plateau. In contrast, the four point pattern was only observed in LLDPE samples drawn at and below 70 °C. As for the HDPEs it persisted into the load−extension curve plateau. The four-point pattern was, however, observed to be less distinct for the LLDPEs than for the HDPE and HMW−HDPE samples. At 90 and 110 °C orientation of the LLDPE (110) orthorhombic reflection proceeded via an equatorially centered arc which decreased in azimuthal extent during deformation. In HDPE, HMW−HDPE, and LLDPE, the four-point pattern was better defined in the annealed compared to the unannealed samples.

Figure 2 contrasts the evolution of the equatorial WAXS peak intensities for unannealed HDPE B and unannealed LLDPE H drawn at 20, 40, 70, 90, and 110 °C. These results are representative of the results for all HDPE (including HMW−HDPE) and LLDPE samples. Since the data were normalized to account for changes in sample thickness, it should be realized that the change in WAXS peak intensities was due to the orientation and amount of crystal phase responsible for the peak. The changes in peak intensities at 40 °C in all samples and at 70 °C for annealed HDPE B were similar to those observed during cold drawing,[33,37] although of a smaller magnitude. There was a sudden decrease in the orthorhombic (110) and (020) intensities, beginning at the yield point and lasting during the postyield drop in load, with the orthorhombic (200) intensity remaining virtually constant. During the load−extension curve plateau the intensities of all the reflections remained constant. The samples for which this behavior was observed were also those in which monoclinic reflections were present, and their behavior has been described more fully previously.[28]

At, and above, 70 °C, however, there was a markedly different type of behavior. Although the orthorhombic (110) and (020) intensities initially decreased in the same manner as for the cold-drawn samples, they subsequently increased while the load dropped, reaching a maximum value during the load−extension curve plateau. As the deformation temperature increased the initial decrease in (110) intensity became progressively smaller and the increase larger. The changes in intensity of all reflections were larger for the HDPE than for the LLDPE, for which the peak intensities remained virtually constant. For both LLDPE and HDPE the magnitude of the changes in peak intensity was less in the annealed samples compared to the unannealed ones. The magnitude of the changes also decreased with decreasing molecular weight.

3.4. SAXS. Two types of behavior were detected by SAXS. The first was the formation of cavities within the necked region at the yield point. In the second, cavitation did not occur and lamellar deformation could be measured throughout deformation.

With the exception of the HMW−HDPE sample E deformed at 70 °C, cavitation was only observed in the samples for which the monoclinic phase was detected by WAXS, and its onset coincided with the appearance of the monoclinic reflections. In sample E, monoclinic reflections were observed in the absence of any measured cavitation.

In the cases where lamellar scattering was measurable throughout deformation, which constituted the HDPE and HMW−HDPE samples drawn at and above 70 °C and the LLDPE samples drawn at all temperatures, the SAXS revealed the transformation from a lamellar to a fibrillar structure. Furthermore, this transformation could be directly correlated with the load−extension curve, as shown in Figure 3. The initial lamellar scattering remained relatively unaltered before

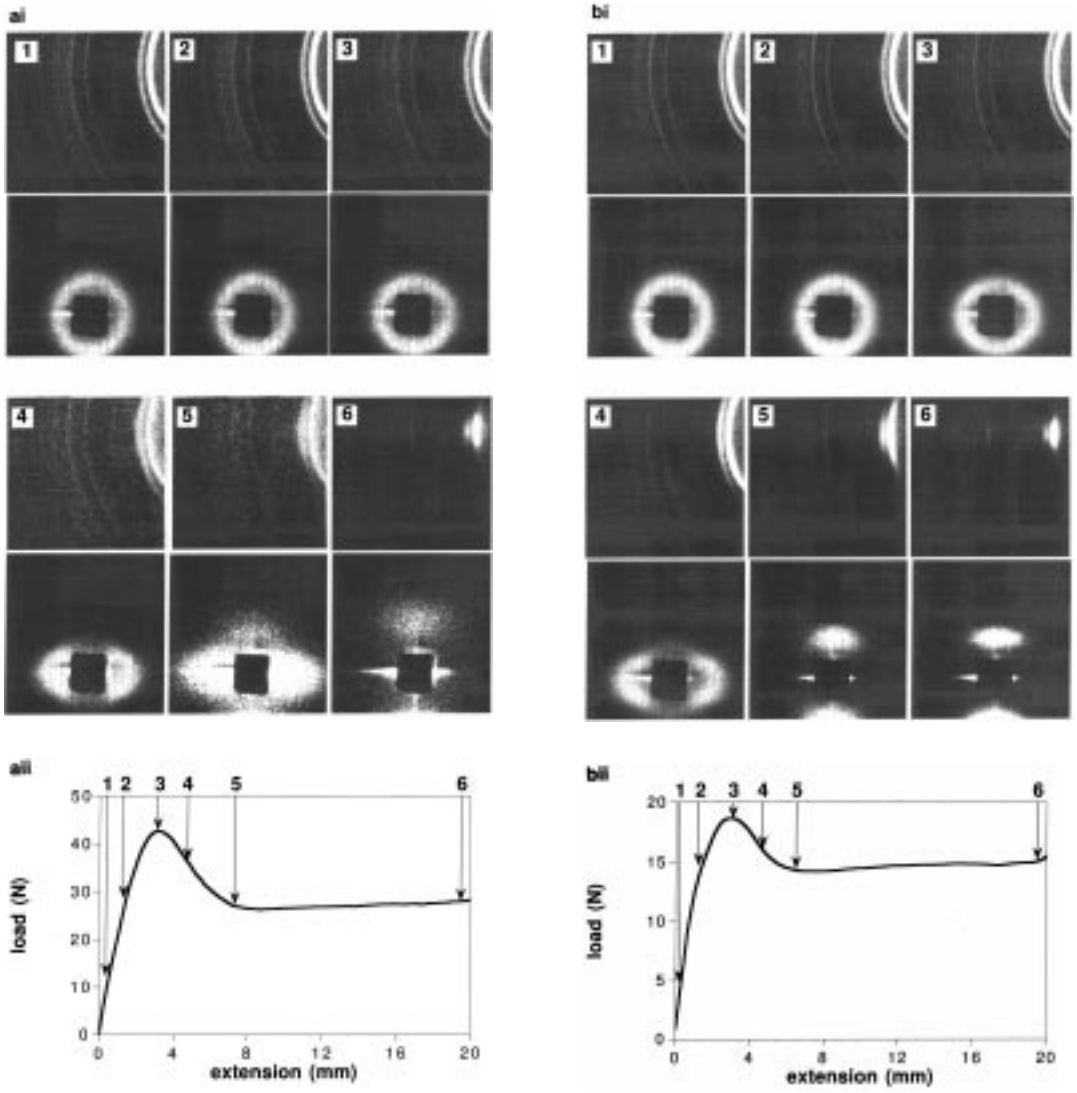

Figure 1. Simultaneously measured WAXS and SAXS patterns (i) and load−extension curve (ii) for unannealed HDPE sample B drawn at (a) 70 and (b) 110 °C.

yield, changing from a circle to an ellipse (with the long axis parallel to the tensile axis (meridian)). However, upon yielding, as shown in the sequences of SAXS patterns in Figure 1, the SAXS became concentrated away from the tensile axis onto the equator. At any particular temperature, the equatorial scattering peak was sharper in the HDPE and HMW−HDPE compared to the LLDPE. After yield, a new peak, with a different long spacing, developed on the meridian while the equatorial lamellar scattering decreased in intensity. In the cases in which there was a postyield drop in load the development of the new meridional long spacing occurred during the drop in load and was complete by the extension at which the load reached a plateau.

At the start of the load−extension curve plateau a well-defined meridional reflection was apparent which subsequently remained unchanged in intensity and profile during deformation but progressively moved to slightly lower scattering angles. This "dash"-shaped meridional pattern was interpreted to result from a well defined fibrillar structure. During the early stages of the load−extension curve plateau the meridional fiber pattern coexisted with the lamellar scattering on the equator, although the latter eventually disappeared completely. Whereas in the HDPE the strain range over which the lamellar and fibrillar morphologies coexisted decreased with increasing deformation temperature, it was found that in the LLDPE a minimum was reached at a temperature of 70 °C, above which the strain range of lamellar and fibrillar coexistence increased again. This observation appeared to be correlated with the fact that above 70 °C the LLDPE samples deformed homogeneously whereas the HDPE samples deformed inhomogeneously.

To demonstrate the correlations between the SAXS and load−extension data, the meridional and equatorial long spacings were measured from the 2D SAXS patterns, as shown in Figure 3. The evolution of the meridional SAXS intensity is shown in Figure 4 for an HDPE and an LLDPE sample, unannealed and annealed, to illustrate the general behavior observed in different types of PE. In all cases the meridional long spacing increased prior to yielding with no change in peak width. During the postyield load drop the lamellar meridional scattering both decreased in intensity and moved to lower long spacings, shown in Figures 3 and 4. At the start of the load−extension curve plateau a new meridional long spacing was established, which corresponded to the periodicity of the fiber structure. Figure 4 shows that the unannealed samples had better

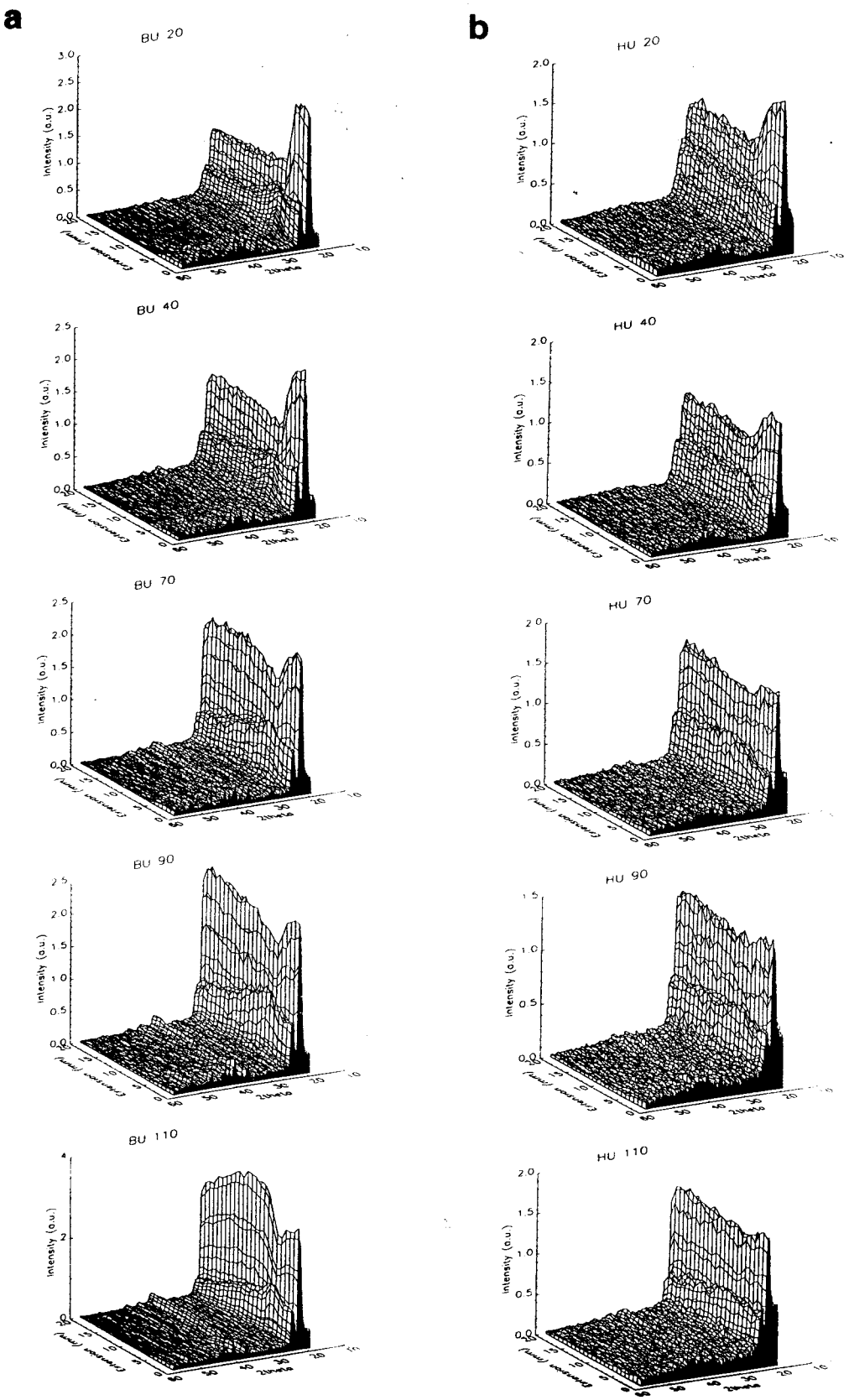

Figure 2. Evolution of the equatorial WAXS intensities for (a) unannealed HDPE sample B and (b) unannealed LLDPE sample H, drawn at the temperatures marked above the figures. The basic similarity between HDPE and LLDPE can be seen, with the greater increase in intensities for the HDPE clearly visible.

defined, more intense, fiber scattering peaks. At any particular temperature there was little difference in peak widths between unannealed samples of different PE types. The annealed LLDPEs, however, had a sharper fiber peak than the annealed HDPE of similar moleculer weight (see Figure 4). As the drawing temperature increased the fiber peak became sharper and moved to higher scattering angles. Table 3 shows the

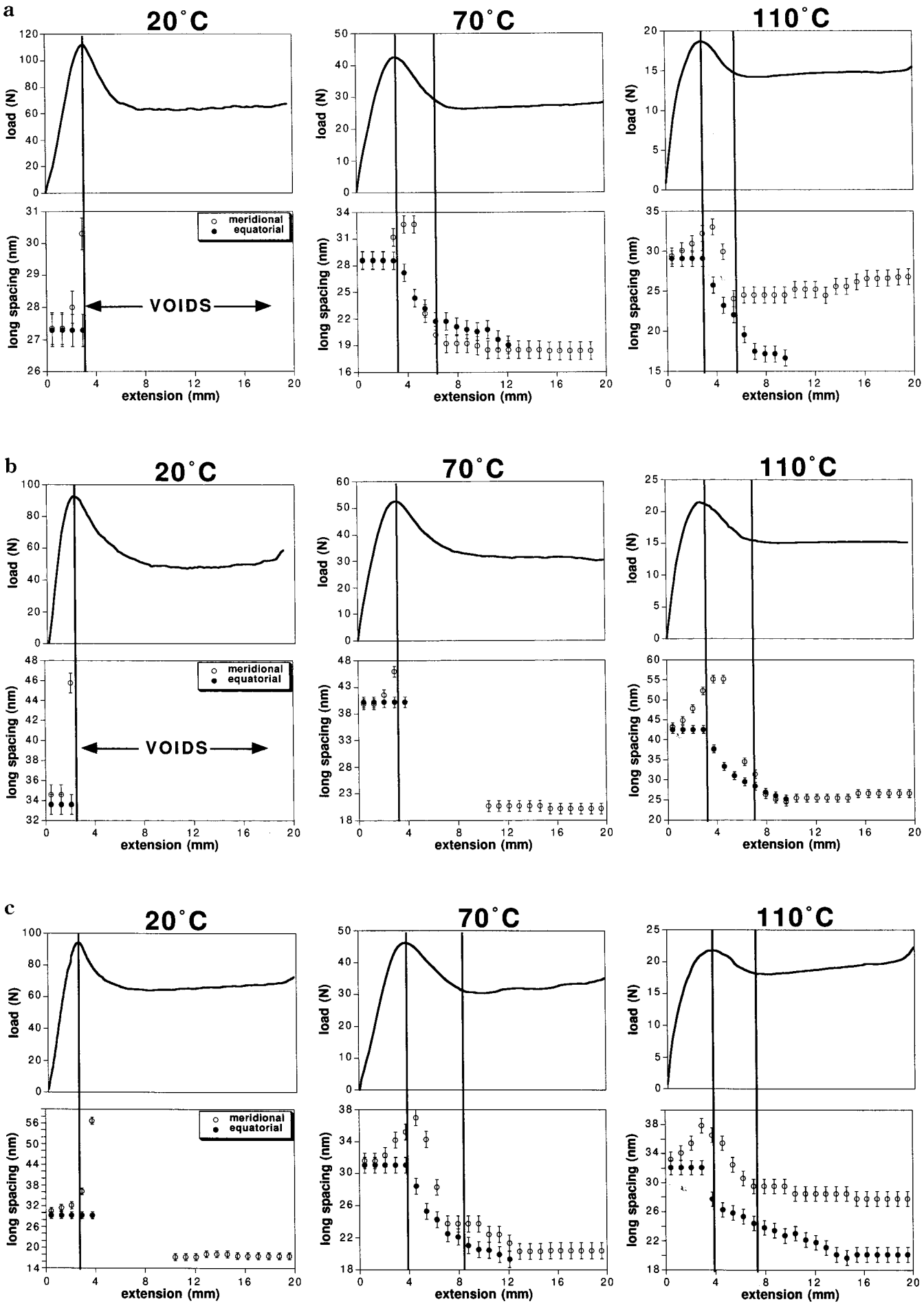
a
20°C
70°C
110°C
load (N)
long spacing (nm)
extension (mm)
meridional
equatorial
VOIDS
b
20°C
70°C
110°C
load (N)
long spacing (nm)
extension (mm)
meridional
equatorial
VOIDS
c
20°C
70°C
110°C
load (N)
long spacing (nm)
extension (mm)
meridional
equatorial

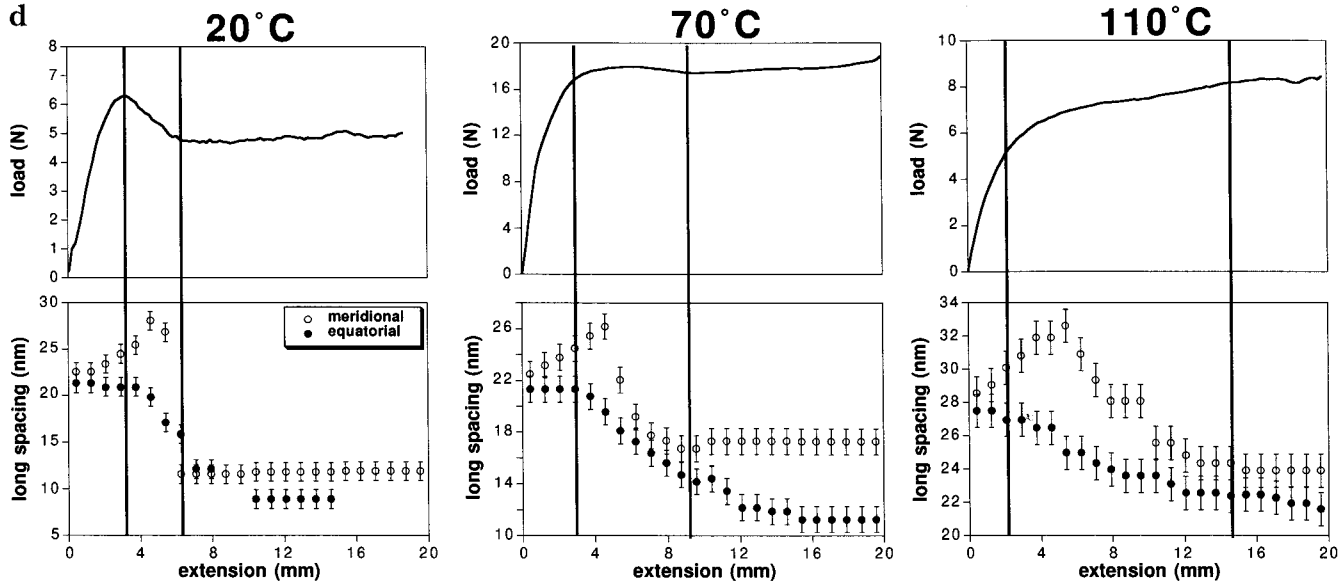

Figure 3. Correlation between the load−extension curve (top) and SAXS equatorial and meridional long spacings (bottom) for (a) unannealed HDPE sample B, (b) annealed HDPE sample B, (c) unannealed HMW−HDPE sample E and (d) unannealed LLDPE sample H. Parts a and b compare the effect of percentage crystallinity, parts a and c compare the influence of molecular weight, and parts a and d compare the effect of branching on the deformation.

values of the fiber long spacing for all of the samples at different temperatures. The fiber long spacing at a particular temperature appeared to be independent of thermal history but increased slightly with increasing molecular weight. The presence of branches (both amount and type) also appeared to have no effect on the value of the fiber long spacing, with the LLDPEs registering similar values to each other and to the HDPEs.

Unlike the meridional long spacing, the equatorial long spacing remained constant during elastic deformation (see Figure 3), accounting for the increasing ellipticity of the SAXS lamellar scattering shown in Figure 1. At the yield point the equatorial long spacing began to decrease. The onset of this decrease (hence the yield point) decreased with increasing deformation temperature. The decrease continued into the load−extension curve plateau. From Figure 5, in which the evolution of the equatorial SAXS profile is shown for an LLDPE sample (in both annealed and unannealed states) drawn at 70 and 110 °C, it can be seen that the equatorial SAXS intensity distribution also changed during deformation, with an increase in scattering at higher scattering angles with increasing strain. A greater increase was registered at lower strains for samples drawn at lower temperatures. The percentage reduction in equatorial long spacing, calculated from the long spacings before and after deformation (to the same extension), shown in Figure 6 for HDPE was found to increase with increasing deformation temperature whereas the opposite trend was observed for LLDPE, shown in Figure 7. The equatorial long spacing finally disappeared at the point at which all traces of lamellar scattering disappeared from the 2D SAXS pattern. Lamellar scattering persisted until higher strains for less crystalline samples.

4. Discussion

4.1. Limitations of the Current SAXS/WAXS Technique. To appreciate the amount of information that can be gained from *in situ* experiments with the setup reported in this paper, it is appropriate to include a section devoted to the limitations of the technique in its current form. The first criticism of the setup is that the local stress and strain at the point of the sample where the X-ray beam is targeted has not been measured. Since the relation between strain and displacement is nonlinear (when the neck is active at the center illuminated by the X-ray beam, small extensions will give a large strain and strain rate. After the load drop, the neck is moving into the wider parts of the specimen and the strain at the center may be very small), a comparison of different samples using displacement is strictly inaccurate. Any differences in the shape of the neck in different samples would mean that equivalent displacements may not be equivalent strains. However, the results have shown that clear correlations are observed between the microstructural changes and the load−extension curve: the universal behavior that occurs at the yield point and the general correspondence of the postyield drop in load with the lamellar to fibrillar transition, for example. It is therefore considered that the correlation of the load−extension curve with the SAXS and WAXS data is a useful exercise. The clear trends in mechanical data, which are rationalized in the following Discussion in terms of sample percentage crystallinity, imply that comparison between samples used in this paper is still worthwhile. Presumably because the samples all have the same geometry, they deform in the same way and can therefore be compared. However, it should be emphasized that these comparisons should be treated with some caution.

A second consideration is how much information can be gained from the X-ray scattering patterns. In particular, limitations of the WAXS detector, which have been recognized by other workers,[38,39] should be mentioned. Most importantly, the parallax error that is inherent in the use of a detector with finite depth and the consequent geometric distortion of the WAXS pattern makes quantitative calculation of the peak widths and azimuthal widths impossible. Since only a portion of the WAXS pattern is measured, the percentage

ai

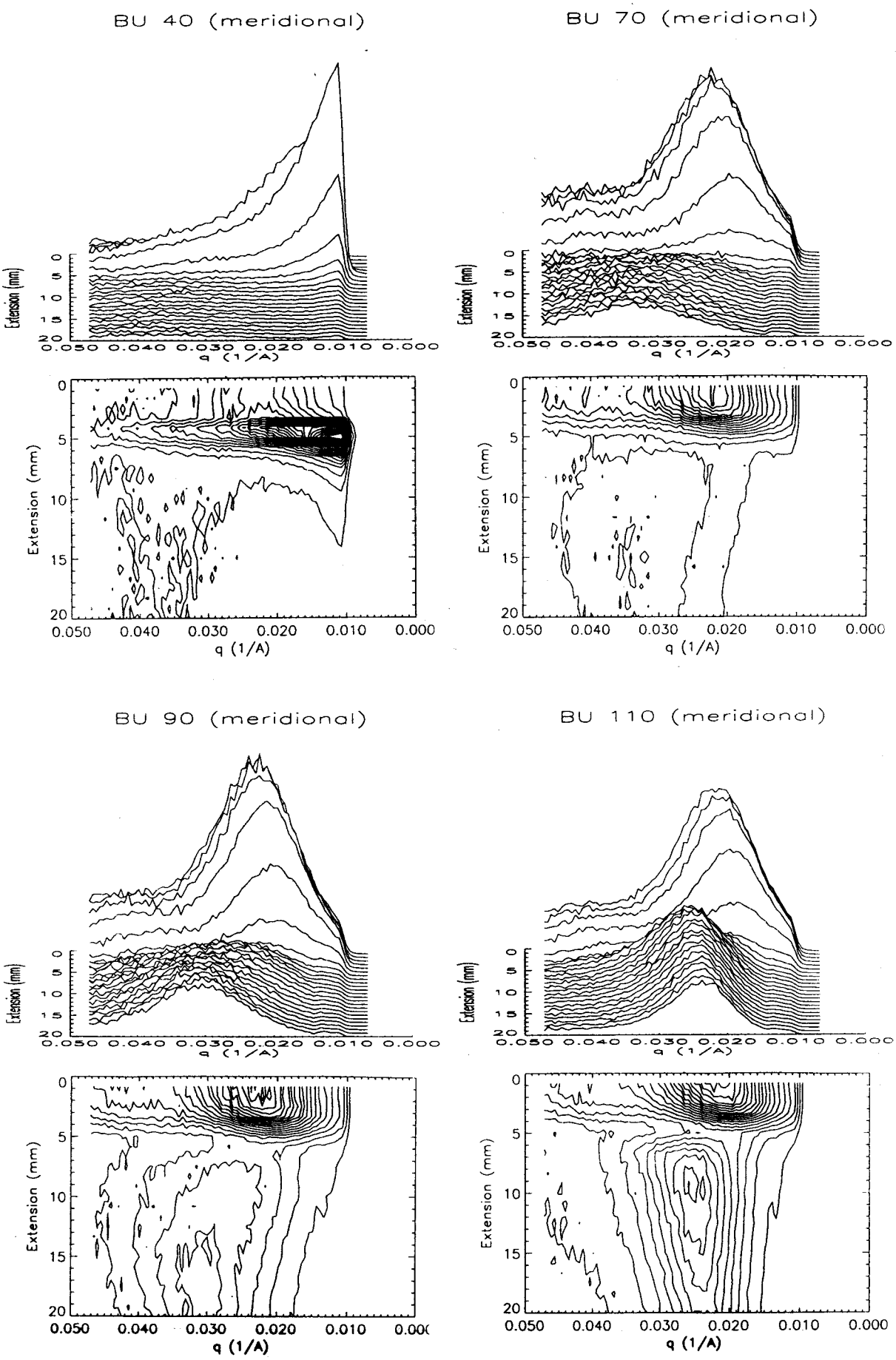
BU 40 (meridional)
BU 70 (meridional)
BU 90 (meridional)
BU 110 (meridional)
Extension (mm)
q (1/A)
0.050 0.040 0.030 0.020 0.010 0.000
0 5 10 15 20

aii

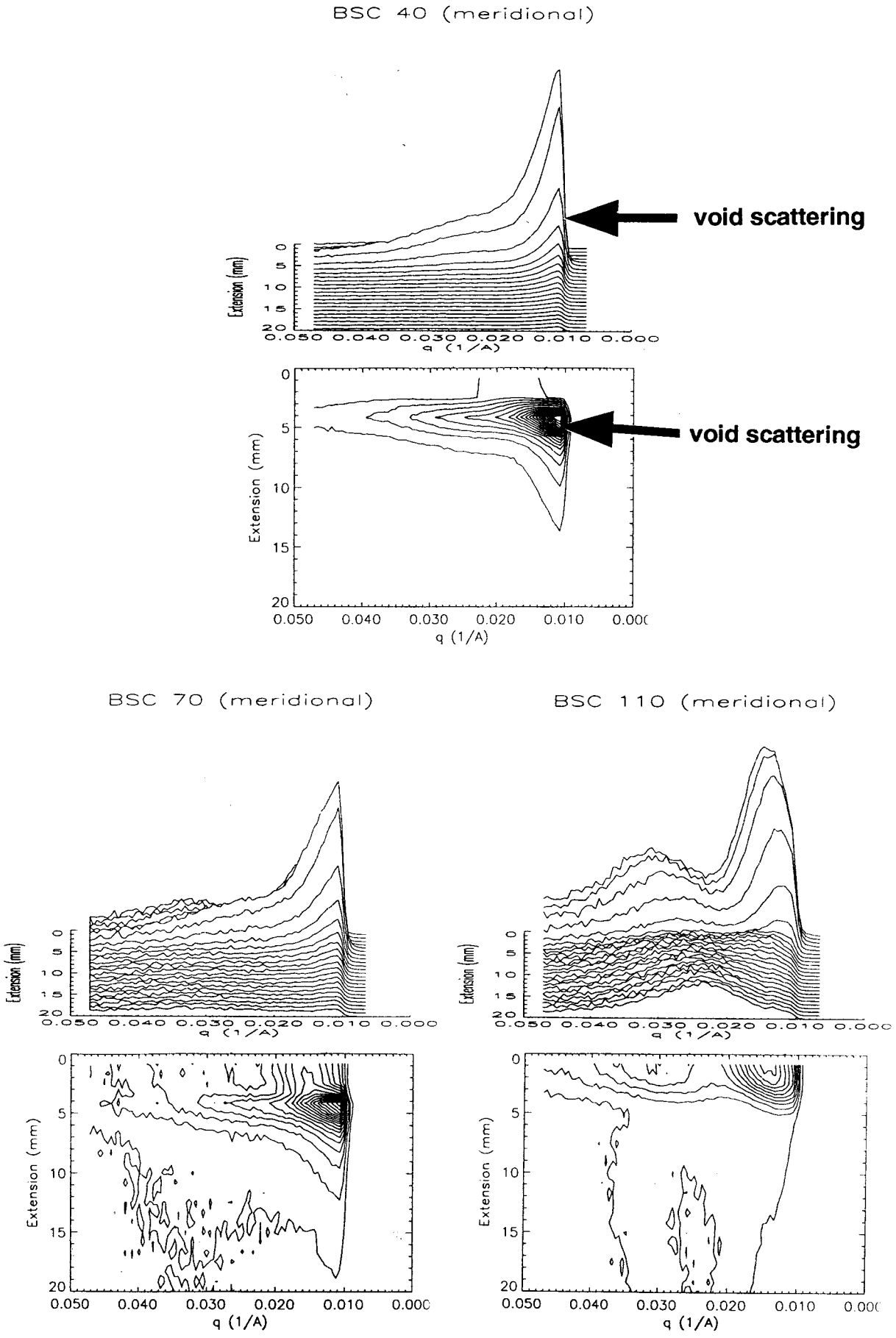
BSC 40 (meridional)
void scattering
void scattering
Extension (mm)
q (1/A)
BSC 70 (meridional)
BSC 110 (meridional)

bi

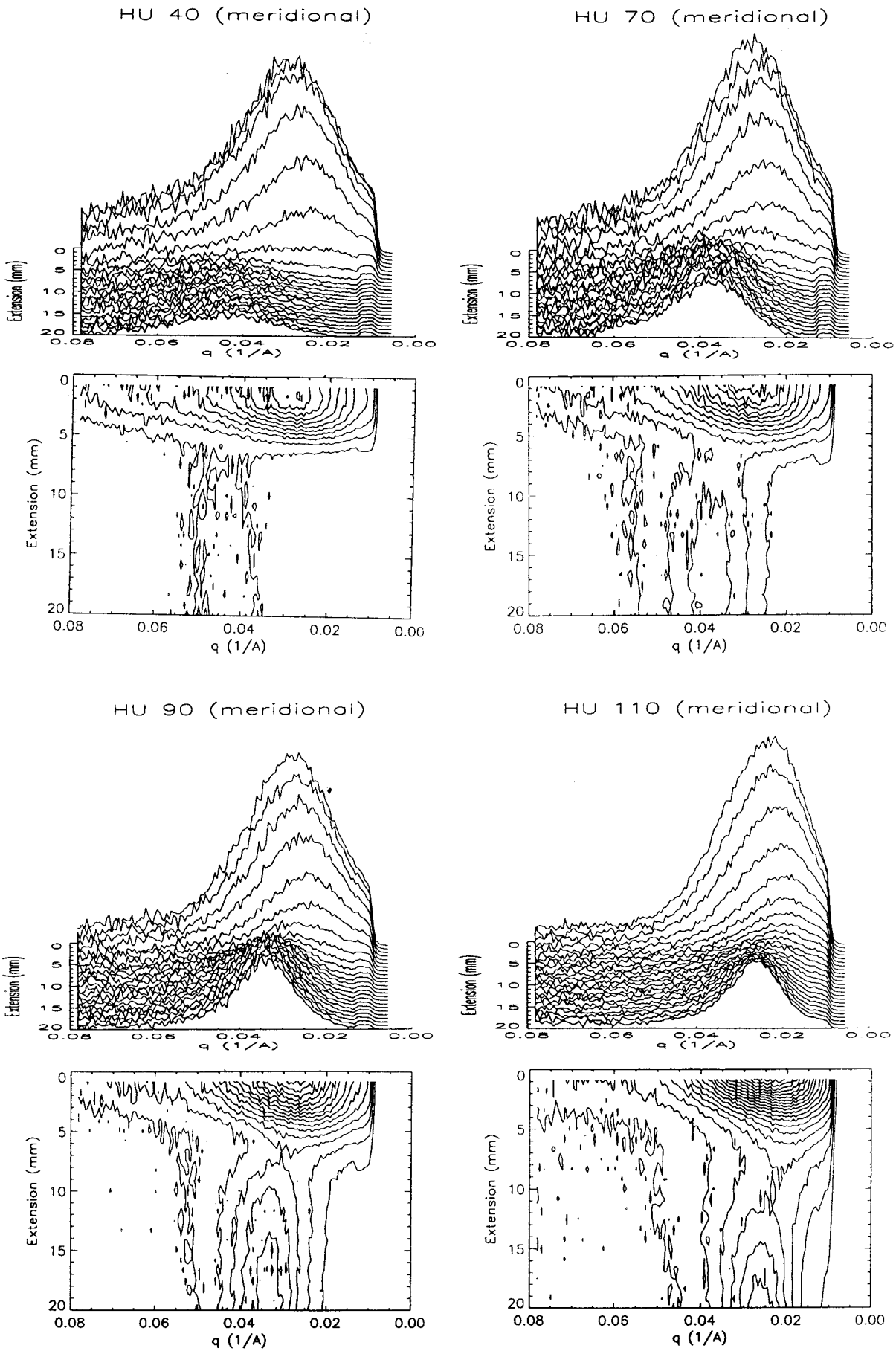
HU 40 (meridional)
HU 70 (meridional)
HU 90 (meridional)
HU 110 (meridional)
Extension (mm)
q (1/A)
0.08
0.06
0.04
0.02
0.00
0
5
10
15
20

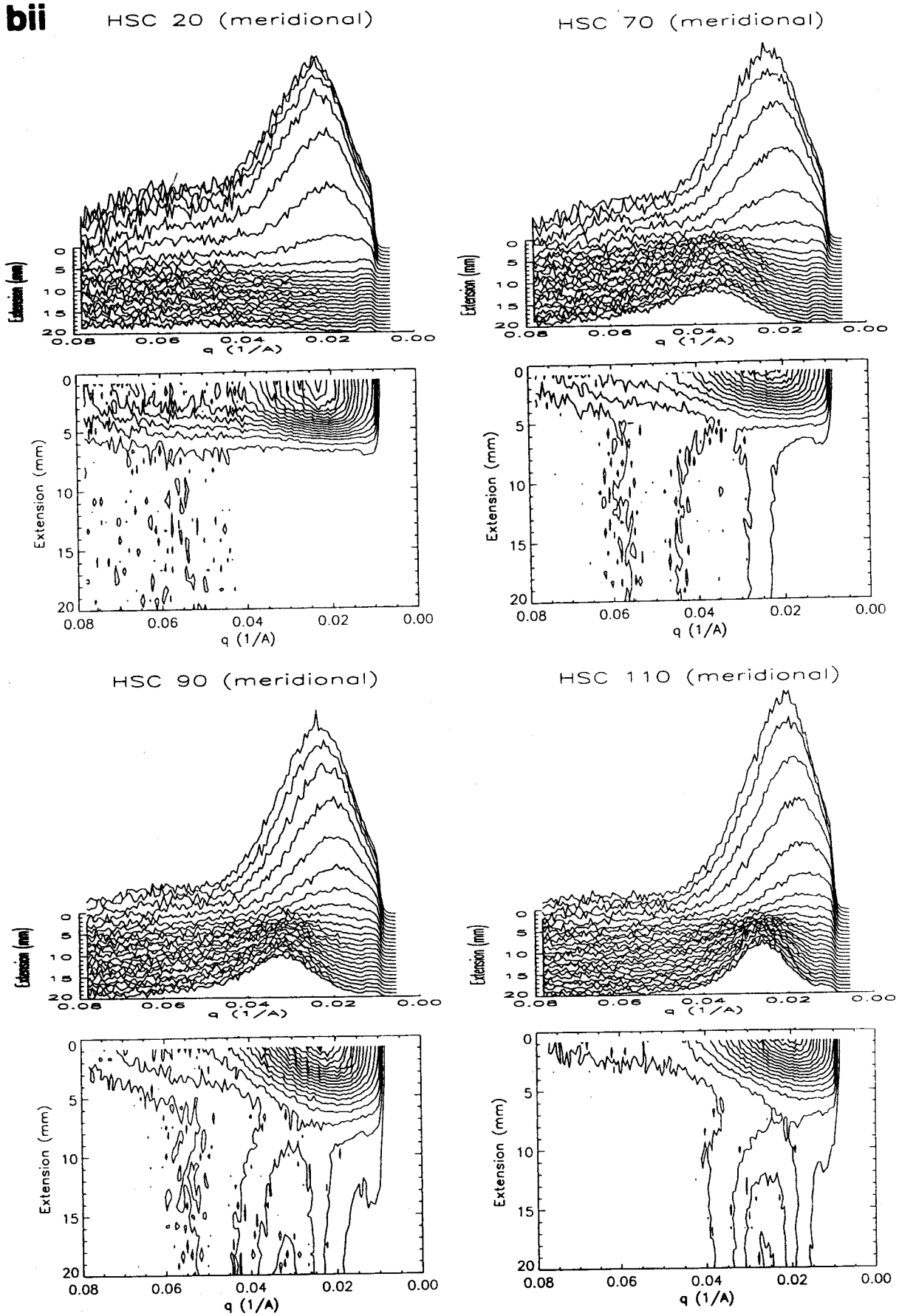

Figure 4. Evolution of the meridional SAXS intensities for (a) unannealed (U) and annealed (SC) HDPE sample B and (b) LLDPE sample H. The signature from voids is indicated for the HDPE sample B where appropriate. The other HDPE samples gave results similar to those for sample B. Likewise, LLDPE samples G and I gave results very similar to those for sample H.

Table 3. Meridional Fiber Long Spacings at Different Drawing Temperatures (Error Approximately ± 1.0 nm)

temp	A		B		E		G		H		I	
(°C)	U	SC	U	SC	U	SC	U	SC	U	SC	U	SC
20	x	x	x	x	x	x	a	a	11.8	11.0	a	a
40	15.9	x	17.2	x	17.5	x	-	-	14.9	-	-	-
70	17.8	17.0	18.6	20.4	20.3	20.1	17.3	17.1	17.3	18.1	16.9	17.9
90	-	-	20.7	-	-	-	-	-	18.6	20.3	-	-
110	24.1	22.7	26.7	25.6	28.2	30.0	-	-	23.9	23.4	23.5	24.2

[a] Key; (x) not measurable (either due to the sample being brittle or, in ductile samples, void scattering overwhelming the fibrillar scattering). (-) sample not run. (a) values may be found in ref 33 for samples of these materials made from different plaques to those used for the series of experiments reported in this paper. The values in ref 33 took the values of approximately 12.0 nm.

crystallinity at different stages of deformation cannot be measured. Therefore, the WAXS data are useful in a qualitative way only: for instance, in the present research it was importantly able to identify a phase transformation by the appearance of additional reflections. A limited quantitative analysis was possible using the peak intensities but only because the scattering was normalized to take into account changes in sample thickness during drawing. Therefore, a decrease in WAXS intensity was due to differences within the structure of the sample rather than there just being less sample present to scatter the X-rays.

Nevertheless, despite the shortcomings, the results (in particular from SAXS and the correlations observed between SAXS/WAXS and the load−extension curve) have shown that simultaneous SAXS/WAXS during drawing can yield useful qualitative and semiquantitative information on the deformation processes in polyethylene. An effort toward improving the current procedures is necessary, however, if the technique is to realize its full potential.

4.2. DSC. The percentage crystallinity, measured by DSC, only decreased in the HDPE samples which cavitated, whereas it increased in the samples in which cavitation was absent. These results suggest that local stress relaxation caused by the voids caused strain-induced decrystallization in HDPE. That a decrease in crystallinity also occurred in HMW−HDPE in the absence of cavitation indicates that cavitation is not the sole cause of relaxation, however. Possibly, a greater proportion of the tie molecules remained intact during deformation in the higher molecular weight samples and enabled them to relax to a greater extent upon release from load, thus destroying any strain-induced crystallinity. It has been found that internal strains are lower in higher molecular weight PE,[40] implying a greater degree of relaxation in these type of samples. The effects are less pronounced in the LLDPE, most probably as a result of the less crystallizable branched chains preventing much strain-induced crystallization from occurring.

4.3. Simultaneous SAXS and WAXS. 4.3.1. Deformation Mechanisms. The evolution of the SAXS and WAXS patterns during cold-drawing has been discussed previously.[28,33,37] Different deformation mechanisms were identified at different stages of deformation for both HDPE and LLDPE. However, the cavitation that occurred at 20 and 40 °C in HDPE prevented the identification of postyield deformation processes and therefore an adequate comparison being made with LLDPE, which did not cavitate at room temperature. The results presented in this paper, in which elevated temperatures reduced and eventually eliminated cavitation, enabled the lamellar deformation to be compared between HDPE and LLDPE. Importantly, they have shown that HDPE and LLDPE experienced a similar sequence of deformation mechanisms. The relative extent of each mechanism was, however, affected by the type of PE.

Preyield deformation in all cases involved the separation of lamellae perpendicular to the tensile axis, which was shown by the increase in meridional long spacing.[5,41−46] The operation of lamellar shear and/or rotation, which is expected to cause little or no alteration in the long spacing of lamellae oriented parallel to the tensile axis, may explain the constant equatorial long spacing. The lack of discernible orientation of the crystalline reflections supports the suggestion that the crystalline phase was involved only to a small extent, or not at all, in deformation prior to yield. It must be emphasized however that since quantitative assessment of the orientation could not be made, these observations were made by detailed inspection only. Therefore, the possibility of some orientation occurring before yield cannot be denied.

The results showed that yielding corresponded to the activation of crystallographic deformation mechanisms in all types of PE at all temperatures, which has been inferred previously from the dependence of the yield stress on the percentage crystallinity.[4,8,47−51] The onset of significant orientation in the crystalline reflections in the WAXS, the activation of the martensitic transformation (in certain samples), and the sudden decrease of the equatorial long spacing in all samples (attributed to chain slip[33,37]) at the yield point, all indicate that crystallographic deformation mechanisms become active at yield. Although the most probable chain slip mechanism is slip on the (100)[001] system, being the mode most easily activated and most commonly identified in unoriented PE,[52−54] the current data were unable to identify this. The activation of chain slip at lower strains in HDPE samples deformed at higher temperatures can be explained by the weakening of the crystals enabling chain slip to occur more readily. Weaker crystals, able to thin to a greater extent, may also account for the larger percentage decrease in equatorial long spacing for the HDPE samples drawn at higher temperatures.

The detection of the monoclinic phase in *in situ* experiments via a stress-induced martensitic tranformation has been discussed in detail in previous publications dealing with the cold-drawing of polyethylene.[28,33,37] Drawing samples over a range of temperatures has confirmed two main influences on the formation of the monoclinic phase. First, the monoclinic phase is formed more readily at lower temperatures, and second, it is formed more readily in more crystalline polyethylenes (the percentage crystallinity may be altered either by thermal history or by the type of polyethylene). Therefore, by increasing the percentage crystallinity it is possible to induce the martensitic transformation at higher drawing temperatures. These results are entirely in accordance with theory; the occurrence of the martensitic transformation is related to the stress experienced by the sample—both decreasing temperature and increasing crystallinity increase the stress and hence promote the formation of the monoclinic phase. However, previous information on the martensitic transformation has mainly been obtained from samples

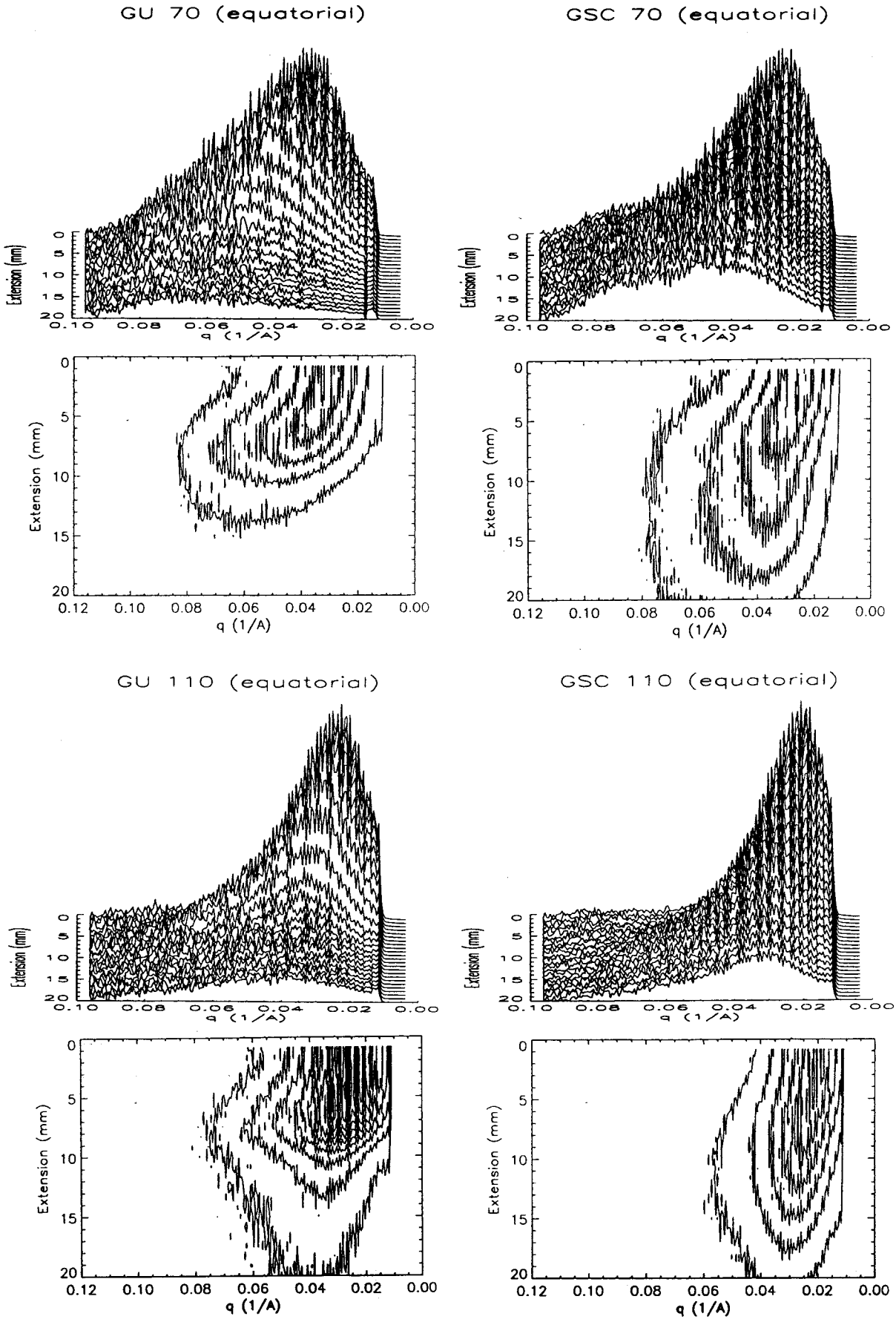

Figure 5. Evolution of the equatorial SAXS intensities for unannealed (left) and annealed (right) LLDPE sample G drawn at elevated temperatures of 70 and 110 °C. The other samples gave similar results.

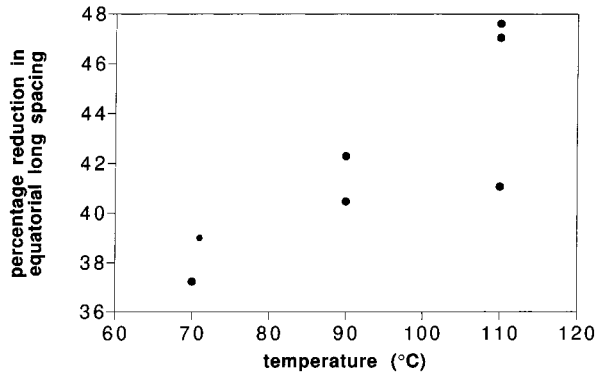

Figure 6. Percentage reduction in equatorial (lamellar) long spacing for HDPE drawn at different temperatures.

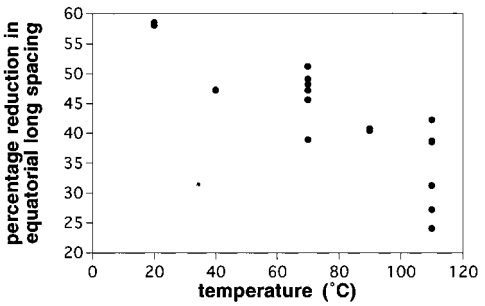

Figure 7. Percentage reduction in equatorial (lamellar) long spacing for LLDPE drawn at different temperatures.

predeformed at a certain temperature, allowed to relax, and then examined at room temperature. Since the monoclinic phase is metastable, existing only under stress,[7] the possibility existed that some monoclinic material formed in these experiments but was able to revert to the orthorhombic form by the time the X-ray experiments were performed. So, although there is nothing unexpected in our finding that the monoclinic phase was not formed at higher temperatures, the current study shows with certainty that it is not. Since the stress state of a sample is determined by its geometry, however, the precise temperatures and crystallinities at which the martensitic transformation was activated in the samples studied in this paper will not necessarily be the same in samples with a different shape. However, although the precise values will not be directly comparable with other literature, the general conclusions remain valid.

It is worth noting the difference in evolution of the peak intensities at different temperatures, even though a quantitative analysis is impossible, since they are related to both orientation and amount of crystal phase present. The previous assertion that the postyield decrease in orthorhombic (110) intensity (which occurred only while the monoclinic phase was forming) was attributed to the conversion of orthorhombic to monoclinic material[28] is supported by the present study which showed that the orthorhombic (110) intensity increased in samples for which the monoclinic phase was absent. An increase in the (110) intensity in these cases may be attributed to the increasing orientation of the molecules causing a concentration of the (110) intensity onto the equator. The initial decrease may be explained by the transient formation of the four-point pattern moving intensity away from the equator. When the martensitic transformation occurred, the increasing orientation of the orthorhombic (110) intensity onto the equator was countered by a decrease in the overall intensity from orthorhombic material due to its conversion into the monoclinic phase.

The immediate postyield deformation has previously been shown, in cold-drawn LLDPE, to be associated with the (continuous) transition from a lamellar to a fibrillar morphology.[33] In cold-drawn HDPE, however, postyield lamellar and/or fibrillar scattering was obscured by the much more intense scattering from a voided structure.[28,37] The results presented in this paper demonstrate that at elevated temperatures for HDPE, when it is possible to observe lamellar and fibrillar scattering, and at all temperatures for LLDPE, the lamellar to fibrillar transition always occurred immediately after the load drop, with the fibrillar morphology always being formed by the onset of the load−extension plateau. The circumstances of the lamellar to fibrillar transition are therefore shown to follow a general behavior.

Increased chain mobility at higher temperatures, possibly involving partial melting, allows for the formation of a more regular fiber structure which would be responsible for the better defined fiber scattering SAXS patterns and more intense SAXS fibre peaks observed at elevated temperatures.[25] The destructive process of a mechanical transformation via shearing and fragmentation may explain the less well-defined fiber structure at lower temperatures.[25] Several previous workers have identified deformation at elevated temperatures with partial melting of less perfect crystallites while stating that at low temperatures the deformation was purely mechanical.[25,55,56] After yield, the lamellar to fibrillar transition coincided with the concentration of SAXS intensity away from the meridian and, with the exception of LLDPE drawn at 110 °C (discussed in the next section), the orthorhombic (110) four-point pattern. Both of these features are associated with tilted lamellae,[57−59] thus suggesting that the lamellae reached an optimum orientation prior to forming the fibrillar morphology. Conversion of the morphology then occurred over a range of strains during which the lamellar and fibrillar morphology coexisted (shown by the coexistence of the equatorial lamellar and meridional fibrillar SAXS). The decrease in lamellar meridional long spacing that occurred during the lamellar to fibrillar transition possibly resulted from lamellar fragmentation, causing a reduction in lamellar thickness.[22]

The increase in cavitation only during the postyield load drop, as a fibrillar morphology is formed, suggests that voids are formed as a result of the release of constraints during lamellar disruption.[2] This hypothesis is in accordance with a mechanical transition causing the lamellar to fibrillar transition at lower temperatures. The suppression of cavitation at elevated temperatures may then result from the increase in chain mobility. At higher temperatures the chains, which are constrained by entanglements and inclusion in the crystalline lamellae, disentangle more readily, and the constraints are overcome without recourse to cavitation. Partial melting at high, but not low, temperatures could also explain the temperature dependence of cavitation.

The slight increase in the meridional SAXS fiber long spacing with increasing strain indicated some elongation of the amorphous material between lamellar fragments. However, most of the deformation in the plateau is likely to occur by drawing new material into the neck,[60,61] and the current results do not yield any information on this region during the load−extension

plateau. They only identify that the fibrillar morphology in the neck remains stable during the portion of the load−extension plateau investigated.

The apparent main dependence of the fiber long spacing on temperature for HDPE and LLDPE may be evidence for the occurrence of melting and recrystallization during the lamellar to fibrillar transition at elevated temperatures.[17,20,25,62−65] However, a mechanical mechanism has been devised which has been used to explain the temperature dependence of the fiber long spacing in terms of the relative amounts of stress-induced crystallization and decrystallization.[22,24,38,66] A larger amount of decrystallization at lower temperatures is held to be the reason for the smaller fiber long spacings measured at lower drawing temperatures. Neverthess, it is not clear that this mechanism would yield long spacings independent of the initial lamellar thickness. If melting had occurred, however, an increase in meridional lamellar long spacing would be expected during the lamellar to fibrillar transition,[67] instead of the experimentally observed decrease. Whether partial melting occurs during deformation therefore remains uncertain.

4.3.2. Effect of Thermal History and Molecular Weight. The differences between the annealed and unannealed samples, and between samples with equivalent thermal histories but different molecular weights, may be interpreted in terms of the relative amounts of inter- and intralamellar deformation that can occur and the influence of tie molecules.[47,68−70] A greater amount of deformation can be borne by the crystalline component in the more crystalline annealed and lower molecular weight samples, explaining the lower strains at which crystallographic deformation was detected in these materials.

The better defined meridional SAXS fiber long spacing in the unannealed samples may be explained by the greater amount of interlamellar material they possess. An increased amount of interlamellar deformation eases the reconstruction of the lamellar morphology to form a more perfect fibrillar structure. Melting is expected to yield a fibrillar morphology independent of the initial lamellar one. Therefore the difference in the degree of perfection of the fibrillar structure between the annealed and unannealed samples supports the role of a mechanical transition from the lamellar to the fibrillar morphologies rather than melting and recrystallization.

4.3.3. Effect of Branching. Although the general progress of deformation observed for LLDPE was the same as for HDPE, there were two noticeable differences: the absence of the four point pattern in the orthorhombic (110) reflection in all LLDPEs drawn at 110 °C, compared to its presence in all other samples and the fact that LLDPE drawn at 110 °C deformed homogeneously whereas the other samples formed a neck. An enhanced amount of interlamellar shear, postulated to occur at elevated temperatures,[2] may explain these observations. It is speculated that intralamellar deformation was dominant at temperatures in the vicinity of 70 °C, resulting mainly in crystallographic and inhomogeneous deformation, but that at higher temperatures interlamellar deformation became dominant, resulting in homogeneous deformation and less crystalline disruption. It is proposed that at 110 °C interlamellar shear combined with chain slip was sufficient to achieve the observed orientation in the LLDPE samples. Such an effect occurred only in the LLDPE samples since they alone possessed sufficient amorphous material to enable enough interlamellar deformation to occur. The operation of interlamellar shear would result in a wider range of lamellar orientations and thus obscure the (110) four-point pattern formed when deformation is mainly crystallographic. Some lamellae did reach the preferred orientation required for lamellar fragmentation, which explains the formation of the fibrillar morphology even though there was no (110) four-point pattern. Other evidence for the increased role of the amorphous component in the LLDPE samples drawn at 110 °C is provided by the smaller reduction in equatorial long spacing at this temperature and the greater strain range over which the lamellar and fibrillar morphologies coexisted, both of which may be explained by a reduced contribution to the deformation from crystallographic slip.

The alternative mechanism of melting and re-crystallization may also be invoked in order to explain the differences between HDPE and LLDPE at 110 °C. Inspection of the DSC traces from the LLDPE samples[33] shows that 110 °C is sufficient to melt the less stable thinner lamellae. Therefore, the (110) four point pattern would not be observed since the fibrillar morphology would be formed, at least partly, by melting and recrystallization rather than tilting of the lamellae to a preferred orientation for mechanical fragmentation. The difference between the HDPE and LLDPE may therefore be because the HDPE samples had melting points approximately 10 °C higher than the LLDPEs, so that 110 °C was not sufficient to reach the melting and recrystallization regime in the HDPE samples, and they always transformed to a fibrillar morphology by mechanical disruption of lamellae. Possibly, HDPE drawn at 120 °C would show a behavior similar to that of LLDPE drawn at 110 °C.

5. Conclusions

A wide variety of polyethylenes have been studied in tension using the technique of simultaneous measurement of the load−extension curve and small-angle and wide-angle synchrotron X-ray scattering. Although possession of local stress−local strain data remains vital, if conclusions are to be drawn which are of most general importance, comparison of samples with the same deformation geometry and their load−extension curves has nevertheless been of some use. Despite reservations as to the usefulness of the load−extension curve for characterizing local deformation, it was shown that the same deformation mechanisms occurred in the same regions of the load−extension curve for all types of PE studied, at all temperatures.

Preyield deformation proceeded via interlamellar separation and possible interlamellar shear and/or rotation. The yield point corresponded to the activation of crystallographic deformation including intralamellar shear and a stress-induced martensitic transformation, favored by low temperatures and higher crystallinities where stresses were higher. Cavitation coincided with the martensitic transformation. Immediate postyield deformation, during which the load decreased in many samples, was associated with the transformation from a lamellar to a fibrillar morphology, the precise details of which were explicable in terms of sample percentage crystallinity. The lamellae appeared to undergo a certain degree of orientation prior to fragmentation into the fibrillar morphology. In LLDPE drawn above 90 °C

a greater degree of interlamellar deformation appeared to be active, resulting in homogeneous deformation, although a fibrillar morphology was still attained (without the drop in load). It is suggested that this effect was only apparent in the LLDPE, since only LLDPE contained sufficient amorphous material for the requisite amount of interlamellar deformation to operate. In general, the behavior of the different polymers could be explained in terms of their different percentage crystallinities enabling different amounts of inter- and intralamellar deformation to operate (a higher percentage crystallinity resulted in more crystallographic deformation). In the case of LLDPE, the short chain branch length had no apparent influence on the mechanical behavior.

Acknowledgment. The help of the following people is gratefully acknowledged: Dr. Elinor Kerr, of BP Chemicals Ltd., Mary Vickers, of the Department of Materials Science and Metallurgy, University of Cambridge, and Peter Bone and Mary Heppenstall-Butler of the Cavendish Laboratory, University of Cambridge. We are particularly grateful for the support of Professor Anthony Ryan, of Sheffield University, throughout these experiments. We are indebted to Elizabeth Towns-Andrews and Dr. Geoffrey Mant, of the CCLRC Daresbury Laboratory, for their technical support which enabled these experiments to be perfomed and for the provision of programs from the CCP13 software suite which were employed in the data analysis. The financial support of the EPSRC and BP Chemicals is acknowledged.

References and Notes

(1) Kennedy, M. A.; Peacock, A. J.; Failla, M. D.; Lucas, J. C.; Mandelkern, L. *Macromolecules* **1995**, *28*, 8. 1407.
(2) Lin, L.; Argon, A. S. *J. Mater. Sci.* **1994**, *29*, 294.
(3) Young, R. J.; Bowden, P. B.; Ritchie, J. M.; Rider, J. G. *J. Mater. Sci.* **1973**, *8*, 23.
(4) Kennedy, M. A.; Peacock, A. J.; Mandelkern, L. *Macromolecules* **1994**, *27*, 5297.
(5) Keller, A.; Pope, D. P. *J. Mater. Sci.* **1971**, *6*, 453.
(6) McConkey, B. H.; Darlington, M. W.; Saunders: D. W.; Cannon, C. G. *J. Mater. Sci.* **1971**, *6*, 572.
(7) Kiho, H.; Peterlin, A.; Geil, P. H. *J. Polym. Sci.* **1965**, *B3*, 157.
(8) Crist, B.; Fisher, C. J.; Howard, P. R. *Macromolecules* **1989**, *22*, 1709.
(9) Popli, R.; Glotin, M.; Mandelkern, L. *J. Polym. Sci., Polym. Phys. Ed.* **1984**, *22*, 407.
(10) Alberola, N.; Cavaille, J. Y.; Perez, J. *Eur. Polym. J.* **1992**, *28*, 949.
(11) Kajiyama, T.; Okada, T.; Sakoda, A.; Takayanagi, M. *J. Macromol. Sci.—Phys.* **1973**, *B7*, 583.
(12) Takayanagi, M.; Kajiyama, T. *J. Macromol. Sci.—Phys.* **1973**, *B8*, 1.
(13) Tanaka, A.; Chang, E. P.; Delf, B.; Kimura, I.; Stein, R. S. *J. Polym. Sci., Polym. Phys. Ed.* **1973**, *11*, 1891.
(14) Peterlin, A. *Advances in Polymer Science and Engineering*; Plenum Press: New York, 1972.
(15) Swan, P. R. *J. Polym. Sci.* **1962**, *56*, 403.
(16) Flory, P. J.; Yoon, D. Y. *Nature* **1978**, *272*, 226.
(17) Popli, R.; Mandelkern, L. *J. Polym. Sci., Polym. Phys. Ed.* **1987**, *25*, 441.
(18) Gent, A. N.; Madan, S. J. *J. Polym. Sci., Polym. Phys. Ed.* **1989**, *27*, 1529.
(19) Juska, T.; Harrison, I. R. *Polym. Eng. Sci.* **1982**, *22*, 766.
(20) Peterlin, A. *J. Mater. Sci.* **1971**, *6*, 490.
(21) Meinel, G.; Peterlin, A. *J. Polym. Sci., Polym. Phys. Ed.* **1971**, *9*, 1967.
(22) Brady, J. M.; Thomas, E. L. *J. Mater. Sci.* **1989**, *24*, 3311.
(23) Vincent, P. I. *Polymer* **1960**, *1*, 7.
(24) Kestenbach, H.-J.; Petermann, J. *Polymer* **1994**, *35*, 5217.
(25) Sadler, D. M.; Barham, P. J. *Polymer* **1990**, *31*, 36.
(26) Sadler, D. M.; Barham, P. J. *Polymer* **1990**, *31*, 43.
(27) Sadler, D. M.; Barham, P. J. *Polymer* **1990**, *31*, 46.
(28) Butler, M. F.; Donald, A. M.; Bras, W.; Mant, G. R.; Derbyshire, G. E.; Ryan, A. J. *Macromolecules* **1995**, *28*, 6383.
(29) Hoffman, J. D.; Davis, G. T.; Lauritzen, J. I. Jr. *Treatise on Solid State Chemistry*, Plenum Press: New York, 1976; Vol. 3.
(30) Wunderlich, B. *Macromolecular Physics*; Academic Press: New York, 1973.
(31) Bliss, N.; Bordas, J.; Fell, B. D.; Harris, N. W.; Helsby, J. I.; Mant, G. R.; Smith, W.; Towns-Andrews, E. *Rev. Sci. Instrum.* **1995**, *66*, 1311.
(32) Bilsborrow, R. L.; Bliss, N.; Bordas, J.; Cernik, R. J.; Clark, G. F.; Clark, S. M.; Collins, S. P.; Dobson, B. R.; Fell, B. D.; Grant, A. F.; Harris, N. W.; Smith, W.; Towns-Andrews, E. *Rev. Sci. Instrum* **1995**, *66*, 1633.
(33) Butler, M. F.; Donald, A. M.; Ryan, A. J. *Polymer* **1997**, *38*, 5521.
(34) Lee, Y. D.; Phillips, P. J.; Lin, J. S. *J. Polym. Sci., Polym. Phys. Ed.* **1991**, *29*, 1235.
(35) Baltà-Calleja, F. J.; Vonk, C. *X-ray Scattering of Polymers*; Elsevier: Amsterdam, 1989.
(36) Butler, M. F. Ph.D. Thesis, University of Cambridge, 1996.
(37) Butler, M. F.; Donald, A. M.; Ryan, A. J. *Polymer* **1998**, *39*, 39.
(38) Hughes, D. J.; Mahendrasingham, A.; Heeley, E. L.; Oatway, W. B.; Martin, C.; Fuller, W. *J. Synchrotron., Radiat.* **1996**, *3*, 84.
(39) Creagh, D. C.; O'Neill, P. M.; Martin, D. J. *J. Synchrotron., Radiat.* **1997**, *4*, 163.
(40) Steidl, J.; Pelzbauer, Z. *J. Polym. Sci.* **1972**, *C30*, 345.
(41) Kaufman, W. E.; Schultz, J. M. *J. Mater. Sci.* **1973**, *8*, 41.
(42) Pope, D. P.; Keller, A. *J. Polym. Sci., Polym. Phys. Ed.* **1975**, *13*, 533.
(43) Peterlin, A.; Meinel, G. *Makromol. Chem.* **1971**, *142*, 227.
(44) Beresford, D. R.; Bevan, H. *Polymer* **1964**, *5*, 247.
(45) Slutsker, A. I.; Sanphirova, T. P.; Yastrebinskii, A. A.; Kuksenko, V. C. *J. Polym. Sci. C* **1967**, *16*, 4093.
(46) Ishikawa, K.; Miyasaka, K.; Maeda, K.; Yamada, M. J. *J. Polym. Sci. A2* **1969**, *7*, 1259.
(47) Brown, N.; Ward, I. M. *J. Mater. Sci.* **1983**, *18*, 1405.
(48) Capaccio, G.; Ward, I. M. *Polymer* **1974**, *15*, 233.
(49) Capaccio, G.; Ward, I. M. *Polymer* **1975**, *16*, 239.
(50) Capaccio, G.; Crompton, T. A.; Ward, I. M. *J. Polym. Sci., Polym. Phys. Ed.* **1976**, *14*, 1641.
(51) Lu, W.; Qian, R.; Brown, N. *Polymer* **1995**, *36*, 3239.
(52) Bartzcak, Z.; Cohen, R. E.; Argon, A. S. *Macromolecules* **1992**, *25*, 4692.
(53) Bartzcak, Z.; Argon, A. S., Cohen, R. E. *Macromolecules* **1992**, *25*, 5036.
(54) Bartzcak, Z.; Argon, A. S.; Cohen, R. E. *Polymer* **1994**, *35*, 3427.
(55) Hoff, M.; Pelzbauer, Z. *Polymer* **1991**, *32*, 999.
(56) Hoff, M.; Pelzbauer, Z. *Polymer* **1992**, *33*, 4158.
(57) Brooks, N. W. J.; Unwin, A. P.; Duckett, R. A.; Ward, I. M. *J. Macromol. Sci.—Phys.* **1995**, *B34*, 29.
(58) Vickers, M. E.; Fischer, H. *Polymer* **1995**, *36*, 2667.
(59) Gaucher-Miri, V.; François, P.; Séguéla, R. *J. Polym. Sci., Polym. Phys. Ed.* **1996**, *34*, 1113.
(60) Rodríguez-Cabello, J. C.; Merino, J. C.; Jawhari, T.; Pastor, J. M. *Polymer* **1995**, *36*, 4233.
(61) Pastor, J. M.; Jawhari, T.; Martin, B.; Merino, J. C. *Colloid Polym. Sci.* **1996**, *274*, 285.
(62) Chuah, H. H.; Lin, J. S.; Porter, R. S. *Macromolecules* **1986**, *19*, 2732.
(63) Bessel, T. J.; Young, R. J. *J. Polym. Sci., Polym. Lett. Ed.* **1974**, *12*, 629.
(64) Corneliussen, R.; Peterlin, A. *Makromol. Chem.* **1967**, *105*, 193.
(65) Corneliussen, R.; Peterlin, A. *J. Polym. Sci. A-2* **1968**, *6*, 1273.
(66) Adams, W. W.; Yang, D.; Thomas, E. L. *J. Mater. Sci.* **1986**, *21*, 2239.
(67) Ryan, A. J.; Bras, W.; Mant, G. R.; Derbyshire, G. E. *Polymer* **1994**, *35*, 4537.
(68) Bartzcak, Z.; Galeski, A.; Argon, A. S.; Cohen, R. E. *Polymer* **1996**, *37*, 2113.
(69) Lu, Z.; Brown, N. *Polymer* **1987**, *28*, 1505.
(70) Lustiger, A.; Markham, R. L. *Polymer* **1983**, *24*, 1647.

MA970681R